Low-Cyclic Fatigue Behavior of Peak-Aged Mg–Nd-Based Alloy

ZHENMING LI, QIGUI WANG, LIMING PENG, ALAN A. LUO, and PENGHUAI FU

In low cycle fatigue, Mg–Nd based alloys exhibit initial cyclic hardening and then softening. The cyclic hardening and softening behaviour of a peak-aged Mg–Nd-based alloy has been studied using transmission electron microscopy. The initial cyclic hardening is attributed to the increase of dislocation density and interaction of dislocations with nano-scale precipitates. The shearing of dislocations through precipitates and the transformation of precipitates in different stages of fatigue are responsible for the cyclic softening. The competing hardening and softening mechanisms present throughout the entire fatigue process. Hardening mechanism dominates in the very beginning of cyclic loading while softening takes over after certain numbers of cycles, say ~ 350 cycles.

I. INTRODUCTION

THE development and application of magnesium alloys, especially Mg-RE (rare earth) alloys with high strength and high toughness, has drawn a great attention in automobile lightweighting.[1,2] Improving fatigue performance of magnesium alloys is one of the most important aspects for wide application of magnesium alloys in automotive structural parts. For magnesium alloys, the key to improving fatigue performance is to clearly understand the deformation mechanism and microstructural evolution during fatigue process. The past research on cyclic deformation mechanisms for magnesium alloys was mainly focused on the twinning and untwinning behavior of wrought magnesium alloys during the low-cycle fatigue process. For instance, the initial {10-12} twinning was reported to affect the plastic deformation mechanism of rolled AZ31 (Mg–3Al–1Zn, all composition is in weight percentage throughout this article unless noted) during fatigue, especially in the stage of compression loading, which can promote the

occurrence of untwinning.[3] Wu et al.[4] analyzed the effect of twinning and slipping on cyclic deformation of an as-extruded AZ31 alloy. Compared with the samples dominated by dislocations-slip mechanism, the fatigue life of those controlled by twin deformation was longer, which is mainly attributed to influence of crack closure induced by surface roughness.[5] The cyclic stress amplitude for the T6-treated (solution treatment at 813 K (540 °C) × 10 hours + aging at 473 K (200 °C) × 14 hours) Mg–3Nd–0.2Zn–1Zr alloy was found to increase at the beginning and then decrease during fatigue for a given strain amplitude,[6] as shown in Figure 1, indicating the cyclic response characteristics of hardening occurred first and softening occurred later.

The variation of cyclic stress is generally related to the evolution of microstructure (precipitates, dislocations and twins). For magnesium alloys, work hardening (such as increase of dislocation density and hindrance of precipitates to dislocation movement) leads to the increase of stress amplitude in the initial cyclic loading stage. Wu et al. studied the relationship between cyclic softening and microstructure of the Mg–10Gd–2.0Zn–0.46Zr alloy during high temperature fatigue, and found that at elevated temperature, grain boundary sliding played an important role in the process of deformation for that alloy. [7] At elevated temperature, grain boundary sliding in magnesium alloys usually occurs because the binding force at the grain boundary decreases. For the age-hardening Al–Mg–Sc alloy, however, cycle softening during low-cycle fatigue is not caused by the stress release after the formation of surface cracks, but by the partial dissolution of Al_3Sc particles.[8] The precipitates in the peak-aged (T6-treated) Mg–3Nd–0.2Zn–0.4Zr alloy are mainly composed of fine and dense shearable β'' ($D0_{19}$) precipitates that

ZHENMING LI is with the Automobile and Motorcycle Parts Research Academy Technology Co., Ltd, Zhejiang Jinfei Kaida Wheel Co., LTD, and Zhejiang Jinyue Machinery Technology Development Co., LTD, Jinghua, 330096, P.R. China. QIGUI WANG is with the General Motors Company, Global Propulsion System, Pontiac, MI 48340. Contact e-mail: qigui.wang@gm.com LIMING PENG is with the National Engineering Research Center of Light Alloy Net Forming and State Key Laboratory of Metal Matrix Composite, Shanghai Jiao Tong University, Shanghai 200240, P.R. China. Contact e-mail: plm616@sjtu.edu.cn ALAN A. LUO is with The Ohio State University, Columbus, OH 43210. PENGHUAI FU is with the National Engineering Research Center of Light Alloy Net Forming, Shanghai Jiao Tong University, Shanghai 200240, P.R. China.
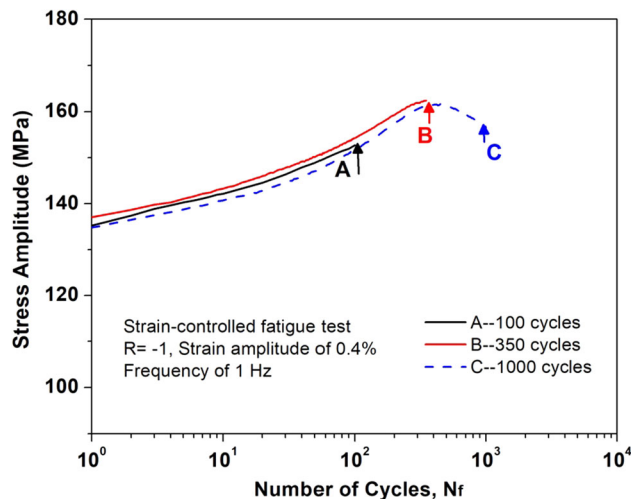
Fig. 1—Variation of cyclic stress amplitude with number of cycles for the T6-treated Mg–3Nd–0.2Zn–1Zr alloy samples tested at a total strain amplitude of 0.4 pct. Curves marked as *A*, *B* and *C* correspond to to 100, 350 and 1000 cycles tested for the samples before transmission electron microscope (TEM) examination.

are coherent with the Mg matrix.[9] Therefore, the cyclic softening in cast Mg alloys containing Nd might also be due to microstructural evolution. The present work is focused on analyzing the microstructure evolution of T6-treated Mg–3Nd–0.2Zn–1Zr alloy during the low cycle fatigue process at room temperature. This paper aims to explore the cyclic deformation mechanisms, the relationship between stress response and microstructure evolution, and in particular, to understand the cause of cyclic softening in cast magnesium alloys containing rare earth (RE) elements.

II. EXPERIMENTAL PROCEDURE

The material used in this work is the Mg–3Nd–0.Zn–1Zr alloy prepared by gravity permanent mold casting process, which has the same chemical composition (Mg–2.99Nd–0.2Zn–0.5Zr) and T6-treated condition (solution treatment at 813 K (540 °C) × 10 hours + aging at 473 K (200 °C) × 14 hours) as reported in Reference 10. Strain-controlled fatigue testing was performed on Instron-8805 fatigue testing machine using a triangle waveform ($R = -1$, frequency of 1 Hz) and total strain amplitude of 0.4 pct. In the present study, the fatigue samples are the same as those reported in Reference 10. The fatigue tests were interrupted after 100 cycles (hardening stage), 350 cycles (corresponding to peak stress) and 1000 cycles (softening stage), respectively. Transmission electron microscope (TEM) samples were cut from the gage length center of the fatigued specimens by electrical discharge machining, ground to 0.2 mm thickness, and electropolished by double spraying (electrolyte of 4 pct perchlorate alcohol, at temperature of 248 K (-25 °C), working voltage of 45 V, and electrical current of 0.2 A). The microstructural evolution during the fatigue process was characterized by a JEM-2100 TEM and an FEI TECNAI G2 20 high resolution projection electron microscope.

III. RESULTS AND DISCUSSION

A. *Evolution of Precipitates During Fatigue*

Figure 2 shows the typical morphologies and corresponding diffraction spots of the precipitates in the T6-treated Mg–3Nd–0.2Zn–1Zr alloy at the initial cyclic hardening stage (100 cycles), peak stress point (350 cycles) and cyclic softening stage (1000 cycles), respectively. The morphology and corresponding diffraction spots of the precipitates in the pre-fatigued sample are included in Figure 2(a) for comparison. The morphology, size and density of the precipitates within samples at different fatigue stages are different. The evolution of the microstructure (especially for the precipitates) corresponds to the change trend of stress response with the increase of numbers of cycles.

Precipitates have been found to form in supersaturated Mg alloys containing Nd during aging.[9–12] The specific aging sequence in Mg–Nd alloys was identified to be: SSSS → ordered G.P.zones (zig–zag shape, $d = 0.37$ nm) → β''(Mg$_3$Nd, hcp, D0$_{19}$, $a = 0.64$ nm and $c = 0.52$ nm, hexagonal prism) → β'(Mg$_7$Nd, orthorhombic, $a = 0.64$ nm, $b = 1.14$ nm and $c = 0.52$ nm, lenticular shape) → β_1(Mg$_3$Nd, fcc, $a = 0.74$ nm, {10–10}$_\alpha$ plate) → β(Mg$_{12}$Nd, tetragonal, $a = 1.03$ nm and $c = 0.59$ nm) → β_e(Mg$_{41}$Nd$_5$, tetragonal, $a = 1.47$ nm and $c = 1.04$ nm).[12] For the T6-treated Mg–3Nd–0.2Zn–1Zr alloy, the precipitates are mainly fine and dispersed β'' on {1–100}$_\alpha$ and {11–20}$_\alpha$ prism planes (marked by yellow arrow in Figure 2(a)).[9] The β'' precipitates (Mg$_3$Nd) are metastable phases and completely coherent with Mg matrix. Other than the fine and dispersed β'' precipitates, some band precipitates (length of 600 to 2000 nm, width of 10 to 50 nm) can also be seen in {1–100}$_\alpha$ prism plane (marked by blue arrows in Figures 2(a) to (b)). Figure 2(c) shows that some of the band precipitates in the T6-treated alloy are cut by the dislocations after 100 cycles (marked by red arrows). Based on relevant References [12–14] and TEM analysis results shown in Figure 2(b), the band precipitates are β_1 precipitates (Mg$_3$Nd) located at {1–100}$_\alpha$ prism plane. However, Nie pointed out that the β_1 precipitates tend to form heterogeneously on preexisting dislocations, resulting in nonuniform distribution of the precipitates.[12] There is no extra reflections for β' precipitates in the diffraction patterns (along [11–20]$_\alpha$ zone axis), so the band precipitates are not considered to be β' precipitates.[13] When the stress amplitude reaches the peak value after 350 cycles, many precipitates (length of 20 to 150 nm, width of 10 to 70 nm) are sheared by dislocations (as shown in Figures 2(d) to (e)), and the number and length of band precipitates decreased remarkably.

In the stage of cyclic softening (*e.g.*, 1000 cycles), the precipitates cut by dislocations at the peak stress point are no longer observed. On the contrary, some other particles, including massive precipitates (marked by
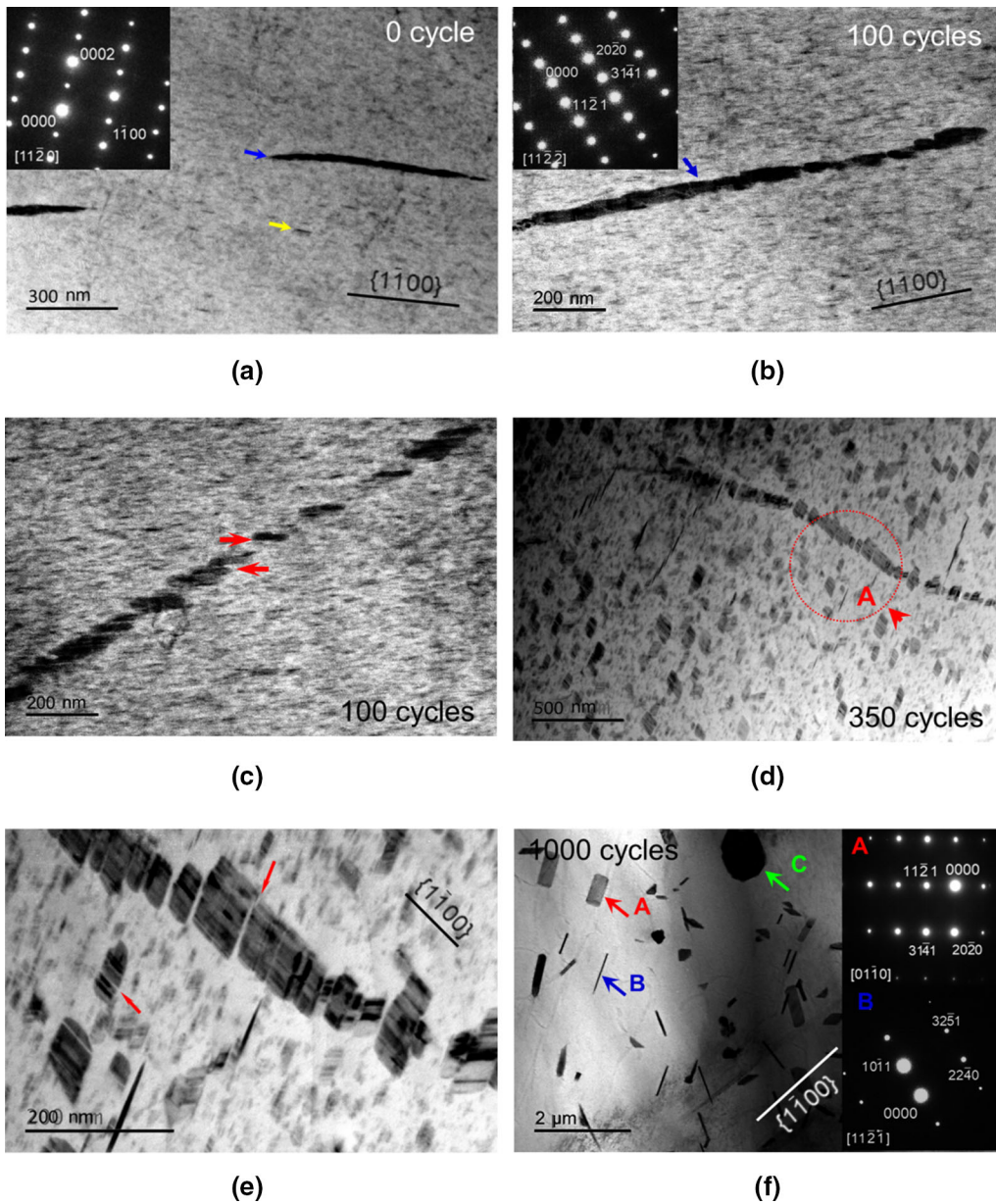
Fig. 2—(a) Bright field image and corresponding diffraction pattern showing the morphology of the precipitates in the pre-fatigued samples (B = $[11–20]_{\alpha}$). (b) Bright field image and corresponding diffraction pattern showing the morphology of the precipitates in the fatigued samples after 100 cycles (B = $[11–20]_{\alpha}$). (c) Some ribbon-shaped precipitates (Nd-rich phases) cut by dislocations after 100 cycles. (d) Bright field image showing the morphology of the precipitates in the fatigued samples after 350 cycles (B = $[11–20]_{\alpha}$). (e) High-magnification image of location A in (d) showing some precipitates cut by dislocations. (f) Bright field image and corresponding diffraction patterns showing the morphology of the precipitates in the fatigued samples after 1000 cycles (B = $[11–20]_{\alpha}$).

arrow A, length of 150 to 1000 nm, width of 100 to 300 nm), rod-like precipitates (marked by arrow B, length of 150 to 1000 nm, width of 40 to 60 nm), and ellipsoid precipitates (marked by arrow C, length of 200 to 1300 nm, width of 200 to 900 nm) with larger size and less quantity have been found (as shown in Figure 2(f)). These precipitates are also located on $\{1–100\}_{\alpha}$ and $\{11–20\}_{\alpha}$ planes. Compared with the band precipitates, the inertia surface and diffraction spots of massive precipitates and ellipsoid precipitates are the same, thus the precipitates with three different shapes are identified to be β_1 precipitates, which have different sizes and

distribution. Furthermore, the rod-like precipitates are considered to be β ($Mg_{12}Nd$) equilibrium precipitation phase. The β phase with a hexagonal shape tend to form as rods and its prism facets are parallel to $\{10–10\}_{\alpha}$.[12] Before the maximum stress amplitude is reached, the number density of the β'' precipitates is decreased while the number density of the β_1 (Mg_3Nd) precipitates gradually increases during cyclic loading. In the cyclic softening stage, the β_1 precipitates gradually decrease, while the β precipitates start to precipitate and coarsen.

Fu et al. pointed out that for the T4-treated alloy in the pre-fatigued state, Zr-containing precipitates (ZrH_2

and Zn–Zr) were formed within grains with different shapes including block-like, globular and rod-like. [15] Figure 3 shows the bright field images for the T4-(solution treatment at 813 K (540 °C) × 10 hours) and T6-treated Mg–3Nd–0.2Zn–1Zr alloy samples after 1000 cycles. For the T4-treated alloy, neither β_1 nor β precipitates were observed after 1000 cycles (as shown in Figure 3(a)), suggesting that in the cyclic softening stage, the β precipitates in the T6-treated alloy (Figure 3(b)) originate mainly from the β_1 precipitates.

B. Morphology of Typical Dislocations and Twins

Figure 4 shows the morphology of typical dislocations observed in the T6-treated alloy after 100 cycles. TEM beam is almost parallel to $[11–20]_\alpha$. Under the conditions of $g = 1–100$ (Figure 4(a)), $g = 1–102$ (Figure 4(b)) and $g = 0001$ (Figure 4(c)), a large number of dislocation bands and dislocation entanglement are observed within grains and near grain boundaries. Figure 4(d) shows the typical dislocation distribution at same location and under the condition of $g = 0002$. Figures 4(e) and (f) indicate the high-magnification images of location A in Figure 4(a) and location B in Figure 4(d), respectively. Dislocations at both the base plane $(0001)_\alpha$ and the non-basal plane are formed.

For the T6-treated alloy, the fine and dispersed β'' precipitates are distributed along $\{1–100\}_\alpha$ and $\{11–20\}_\alpha$ which are perpendicular to $(0001)_\alpha$ slip plan acting as a strong barrier to the basal slip. Cyclic hardening is mainly attributed to the increase of dislocations density caused by dislocation entanglement, shutting down (disappearance) and generation of new dislocation sources. The dislocations can be divided into two types: straight dislocations and curved dislocations (as shown in Figures 4(e to f)). Both types of dislocations at basal and non-basal planes are suggested to be $\langle a \rangle$ dislocations (as shown in Figure 4(e), under the conditions of $g = 1–100$). Non-basal $\langle a \rangle$ dislocations are likely to be non-basal slip between two basal planes. In addition, under the condition of $g = 0002$, the dislocations which are generally considered as $\langle a + c \rangle$ or $\langle c \rangle$ dislocations can be also seen at both basal and non-basal planes (as shown in Figure 4(f)).

Fu et al. pointed out that for the T4-treated NZ30K alloy,[16] apart from the basal and non-basal $\langle a \rangle$ dislocations, $\langle a + c \rangle$ or $\langle c \rangle$ dislocations also participated in the tensile deformation at room temperature. Agnew et al. [17] suggested that for a wrought AZ31 alloy, the plastic forming performance is greatly improved by $\langle a + c \rangle$ non-basal sliding. Moreover, the dislocations with $\langle c \rangle$ vector and dislocations ($\langle a + c \rangle$ or $\langle c \rangle$) are also activated in the solutionized Mg–Li alloy during tensile deformation.[18] The addition of a small amount of Zn to Mg–Nd–Zr alloy can promote the movement of dislocations on non-basal plane and improve the alloy formability.[16] Consequently, the $\langle a + c \rangle$ or $\langle c \rangle$ dislocations are also believed to be able to be activated in the T6-treated Mg–3Nd–0.2Zn–1Zr alloy during fatigue deformation.

It is well known that twinning is also one of the important deformation modes in magnesium alloys. The interaction between twins, precipitates and dislocations is of great significance to the plastic deformation of magnesium alloys, which may change the slip mode and activate the non-basal slip to improve the plastic deformation. In this study, some $\{10–12\}_\alpha$ twins near the grain boundaries (as shown in Figures 5(a) to (b)) and within grains (as shown in Figures 5(c) to (d)) are observed in the T6-treated alloy after 350 cycles of cyclic loading. However, no twins are observed in the samples after 100 or 1000 cycles. In the early stage of cyclic loading (e.g., 100 cycles), the activation of the dislocations at basal and non-basal planes leads to the deformation, and the twinning is not required. When the strain hardening reaches to peak (e.g., 350 cycles), it is difficult to coordinate deformation by
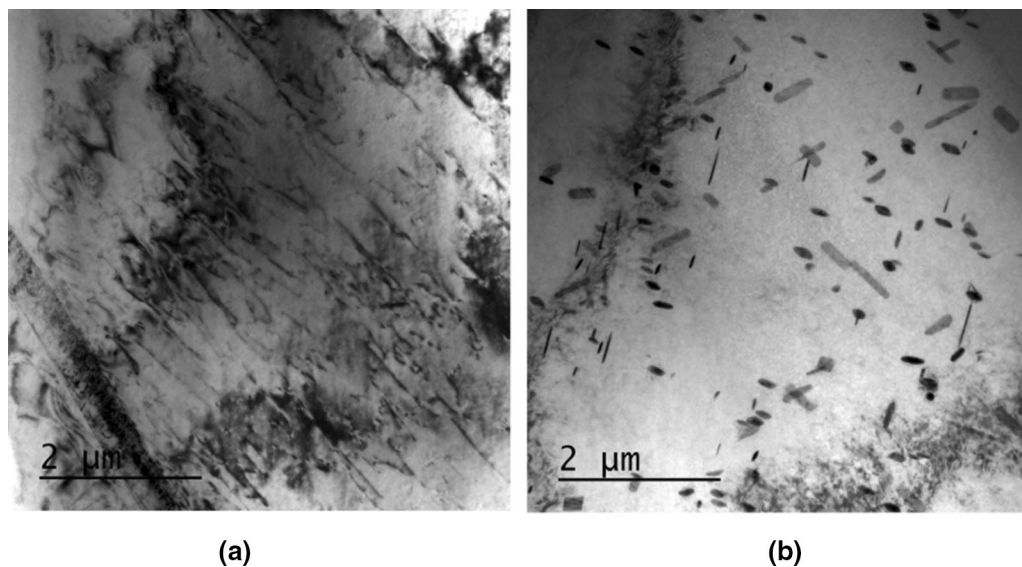

(a)   (b)

Fig. 3—Bright field images showing typical microstructure and β precipitate morphology in (a) T4- and (b) T6-treated alloys after 1000 cycles.
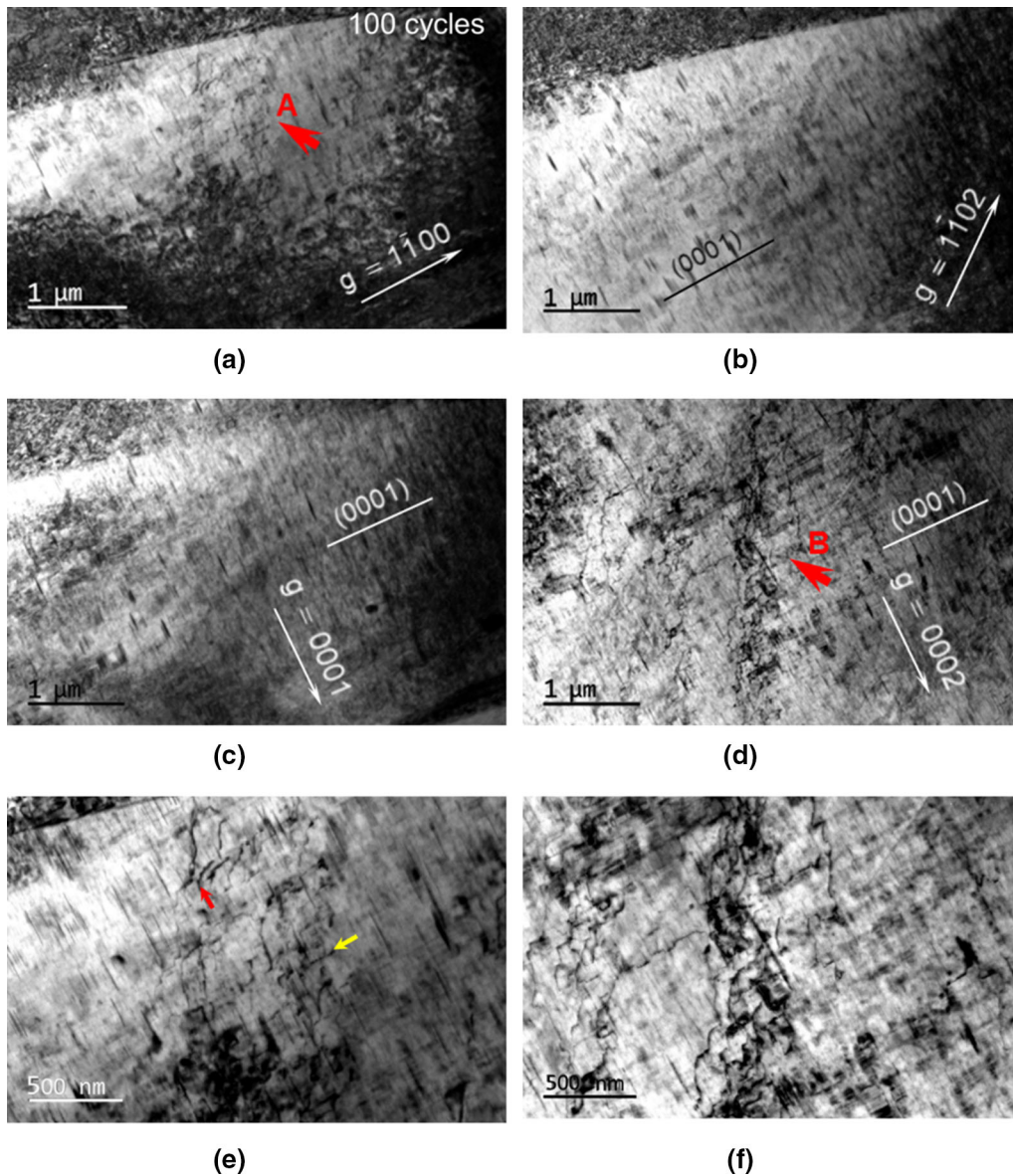
Fig. 4—(a) Bright field images of the T6-treated Mg–3Nd–0.2Zn–1Zr alloy samples tested at a strain amplitude of 0.4 pct after 100 cycles (B = [11–20]$_\alpha$, g = 1–100). Typical dislocation distribution at the same location and different base vectors ((b) g = 1–102, (c) g = 0001 and (d) g = 0002). High-magnification images of (e) location A and (f) location B showing the configuration of the typical dislocations.

dislocations-slip alone. Twinning can change the orientation of the crystal and make the dislocation easy to slip.

Furthermore, as shown in Figure 5(a), a large number of dislocations are formed between twins and grain boundaries. Both twin and grain boundaries would hinder dislocation movement. Twinning can cut off the originally continuous slip system, which increases the difficulty of dislocation movement. Figure 5(b) shows the interaction mechanism between twins, precipitates and dislocations. A large number of the dislocations are activated in {10–12}$_\alpha$ twins. The local stress concentration in the twins leads to the formation of the dislocations when the dislocations cross the twin boundary. The precipitates also hinder the movement of dislocations at the twin interface and inside twins. In addition, it can be seen from Figure 5(d) that some twins (marked by yellow arrows) and precipitates (marked by red arrows) were cut by the dislocations. The precipitates affect the nucleation and growth of twinning, because they would pin a twin interface and restrict the movement of a twin boundary, thus constraining the twin growth. When the cycle time is continuously increased (i.e., 1000 cycles), the matrix strength of the alloy is obviously reduced while the plasticity is improved due to the transformation of the precipitates. The dislocations-slip can satisfy the requirement of cyclic plastic deformation and the need for twinning to contribute to the required plasticity is significantly decreased.

Fig. 5—(*a*) Bright field image and corresponding diffraction pattern showing twin (marked by yellow arrow) near the grain boundaries, precipitates (marked by red arrow) and dislocations (marked by blue arrow) in the fatigued samples after 350 cycles (B = [11–20]$_\alpha$). (*b*) High-magnification image for (a) showing the relationships between twin, precipitates and dislocations in the samples. (*c*) Bright field image showing the precipitates and twin within grains of the samples after 350 cycles. (*d*) High-magnification image for (c) showing that the twin (marked by yellow arrows) and precipitates (marked by red arrows) cut by dislocations (Color figure online).

C. *Shearing Mechanism of Precipitates by Dislocations*

Figure 6(a) indicates that the precipitates in the T6-treated samples after 350 cycles are mainly composed of β'' precipitates (marked by the yellow arrow) and β_1 precipitates (marked by the blue arrow). It can be seen that these precipitates are mainly distributed along $\{1{-}100\}_\alpha$ plane. For the T6-treated alloy, the increase of cycle time leads to the increase of number density and segregation of dislocations. The accumulation of dislocations around the β'' precipitates and the entanglement of dislocations (as shown in Figure 6(b)) leads to great stress–strain field, which promotes the phase transformation from metastable β'' precipitates to β_1 precipitates and the aggregation growth of the precipitates.[19–22] In addition, the increased stress–strain field also provides a basis for dislocations to cut through the shearable precipitates.

The dark field image as shown in Figure 6(c) further confirms that the parallel straight lines perpendicular to the growth direction of the precipitates are the dislocations rather than the precipitates. The bright field image shown in Figure 6(d) indicates that the precipitates can block the movement of the dislocations. In the present work, the lattice structure of dislocations and the mechanisms of the precipitates sheared by dislocations during fatigue are described using high-resolution bright field image (Figure 6(e)) and dark field image (Figure 6(f)). The lattice distortion caused by the

dislocations blocked by the precipitates can be observed. Furthermore, it is seen from Figure 7 that shear occurs on the surface of local position of β'' precipitates, resulting in the change of the surface structure.

In addition to slip on basal plane, the dislocations mainly slip on $\{11{-}20\}_\alpha$ and $\{1{-}100\}_\alpha$ prism planes, and the directions of slip are considered as $\langle 11{-}20\rangle_\alpha$ and $\langle 1{-}100\rangle_\alpha$, respectively. The metastable precipitates (β'' and β_1) are affected by two aspects during fatigue. On the one hand, the precipitates can be sheared repeatedly by dislocations. After the precipitates are initially sheared, the effective area of the precipitates decreases, which would make the subsequent shear of the precipitates easier. With the combined effect of cyclic straining and stress concentration at the interface between precipitates and matrix, the metastable β_1 precipitates gradually transform to the final equilibrium β precipitates.

IV. CONCLUSIONS

For the T6-treated Mg–3Nd–0.2Zn–1Zr alloy, the cyclic stress initially increases followed by a decrease during the fatigue process, which is attributed to the competitive mechanisms between cyclic hardening and cyclic softening. In the early stage of fatigue deformation, the density of dislocations increases and β'' and β_1 precipitates interact with dislocations, which would lead
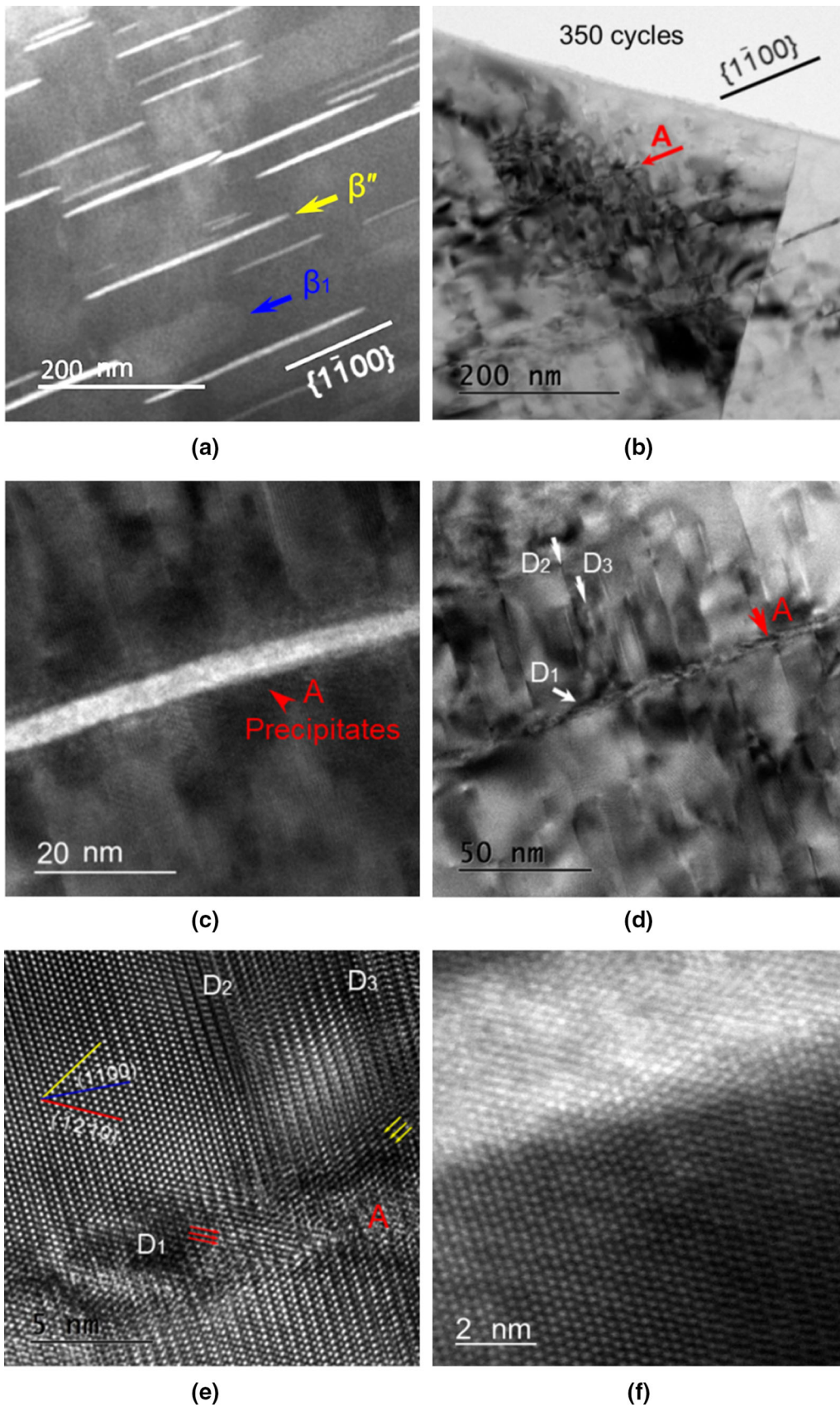
Fig. 6—(a) STEM image showing the morphology of the precipitates in the T6-treated samples after 350 cycles. (b) Bright field image showing the precipitates and dislocations in the alloy after 350 cycles. High-magnification images under (c) dark field and (d) bright field for location A in (b). High-resolution images under (e) bright field and (f) dark field showing the precipitates and the dislocations (D_{1-3}) near the precipitates.
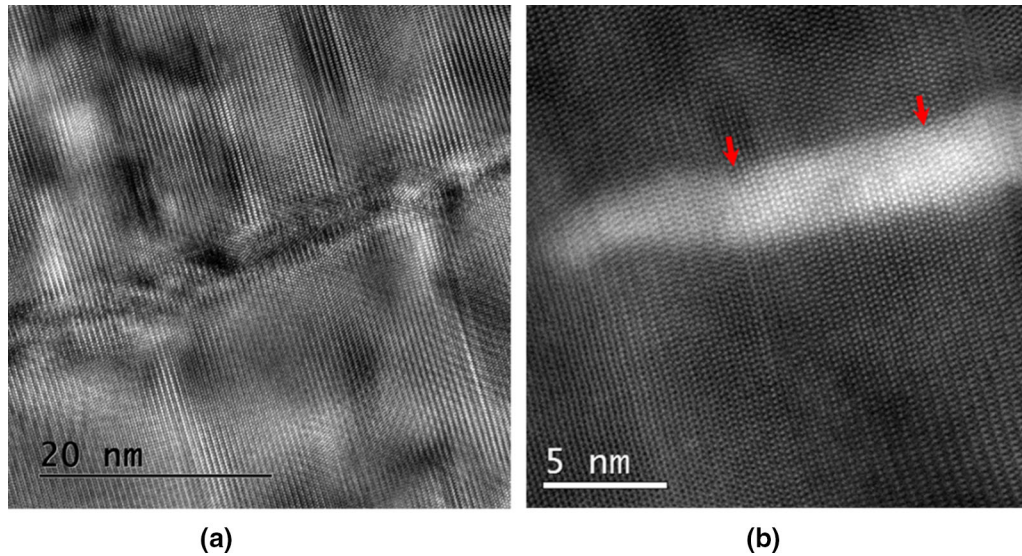
Fig. 7—(*a*) Bright field image and (*b*) dark field image showing the relationship between precipitates and dislocations in the T6-treated samples after 350 cycles.

to cyclic hardening. Meanwhile, β'' precipitates start to transform to β_1 precipitates, resulting in cyclic softening. It appears that the cyclic hardening is much stronger than the cyclic softening during this stage. With the increase of cycle time from 350 to 1000 cycles, the metastable β_1 precipitates start to transform to β precipitates, which leads to the cyclic softening.

ACKNOWLEDGMENTS

REFERENCES

1. W.J. Joost and P.E. Krajewski: *Scripta Mater.*, 2017, vol. 128, pp. 107–12.
2. S.M. Zhu, M.A. Easton, T.B. Abbott, J.F. Nie, M.S. Dargusch, N. Hort, and M.A. Gibson: *Metall. Mater. Trans. A*, 2015, vol. 46A, pp. 3543–54.
3. S.H. Park, S.G. Hong, and C.S. Lee: *Scripta Mater.*, 2010, vol. 62, pp. 202–05.
4. Y.J. Wu, R. Zhu, J.T. Wang, and W.Q. Ji: *Scripta Mater.*, 2010, vol. 63, pp. 1077–80.
5. S. Suresh and R.O. Ritchie: *Metall. Trans. A*, 1982, vol. 13, pp. 1627–31.
6. Z.M. Li, A.A. Luo, Q.G. Wang, L.M. Peng, and P. Zhang: *Metall. Mater. Trans. A*, 2016, vol. 47A, pp. 4239–57.
7. L.Y. Wu, Z. Yang, W.J. Xia, Z.H. Chen, and L. Yang: *Mater. Des.*, 2012, vol. 36, pp. 47–53.
8. C. Watanabe, R. Monzen, and K. Tazaki: *Int. J. Fatigue*, 2008, vol. 30, pp. 635–41.
9. P.H. Fu, L.M. Peng, H.Y. Jiang, J.W. Chang, and C.Q. Zhai: *Mater. Sci. Eng. A*, 2008, vol. 486, pp. 183–92.
10. Z.M. Li, Q.G. Wang, A.A. Luo, P. Zhang, and L.M. Peng: *Metall. Mater. Trans. A*, 2016, vol. 47A, pp. 2686–2704.
11. D.H. Ping, K. Hono, and J.F Nie: *Scripta Mater.*, 2003, vol. 48, pp. 1017–22.
12. J.F. Nie: *Metall. Mater. Trans. A*, 2012, vol. 43, pp. 3891–939.
13. J.J. Bhattacharya, F. Wang, P.D. Wu, W.R. Whittington, H.E.I. Kadiri, and S.R. Agnew: *Int. J. Plasticity*, 2016, vol. 81, pp. 123–51.
14. L. Ma, R.K. Mishra, M.P. Balogh, L.M. Peng, A.A. .Luo, A.K. Sachdev, and W.J. Ding: *Mater. Sci. Eng. A*, 2012, vol. 543, pp. 12–21.
15. P.H. Fu, L.M. Peng, H.Y. Jiang, C.Q. Zhai, X. Gao, and J.F. Nie: *Mater. Sci. Forum*, 2007, vols. 546–549, pp. 97–100.
16. P.H. Fu, L.M. Peng, J.F. Nie, H.Y. Jiang, L. Ma, and L. Bourgeois: *Mater. Sci. Forum*, 2011, vol. 690, pp. 230–33.
17. S.R. Agnew and O. Duygulu: *Int. J. Plasticity*, 2005, vol. 21, pp. 1161–93.
18. S.R. Agnew, J.A. Horton, and M.H. Yoo: *Metall. Mater. Trans. A*, 2002, vol. 33, pp. 851–58.
19. J. Lendvai, H.J. Gudladt, and V. Gerold: *Scr. Metall.*, 1988, vol. 22, pp. 1755–60.
20. B. Skrotzki, G.J. Shiflet, and E.A. Starke, Jr.: *Metall. Mater. Trans. A*, 1996, vol. 27A, pp. 3431–44.
21. D.Y. Li and L.Q. Chen: *Acta Mater.*, 1998, vol. 46, pp. 2573–85.
22. X.Y. Liu, Q.L. Pan, X.L. Zhang, S.X. Liang, L.Y. Zheng, F. Gao, and H.L. Xie: *Mater. Des.*, 2014, vol. 58, pp. 247–51.